Research Article

Fitri Nur Kayati, Chandra Wahyu Purnomo*, Yuni Kusumastuti, and Rochmadi

The optimization of hydrogel strength from cassava starch using oxidized sucrose as a crosslinking agent

https://doi.org/10.1515/gps-2023-0151
received August 11, 2023; accepted November 15, 2023

Abstract: The mechanical properties of hydrogels are crucial in wound dressing application. Starch-based hydrogels have deficiencies in mechanical strength and gel stability. These shortcomings can be addressed by employing crosslinking techniques with oxidized sucrose. A design of experiments approach was used to optimize the tensile strength of the product. The results indicated that both the composition of oxidized sucrose and glycerol significantly impact tensile strength (p-value < 0.05). The optimal tensile strength achieved was 27 MPa, using 0.9762 mL of oxidized sucrose and 0.0624 g of glycerol per gram of starch. The hydrogel products underwent a series of characterizations, including optical microscope examination, Fourier Transform Infrared Spectroscopy (FTIR), Proton Nuclear Magnetic Resonance (^{1}H NMR), swelling test, Water Vapor Transmission Rate (WVTR), contact angle, and cytotoxicity test. The FTIR and ^{1}H NMR analyses confirmed the crosslinking of hydroxyl groups within starch molecules with aldehyde groups from oxidized sucrose. Characterization of this hydrogel revealed that it had a swelling capacity of 95%, a WVTR of 714.92 g per m^2 per 24 h, a contact angle of 74.76°, and a cell viability value greater than 100%. Thus, this hydrogel is suitable for wound dressing due to its strength, exudate-absorbing capabilities, moisture retention properties, hydrophilicity, and non-toxicity.

Keywords: hydrogel film, starch, oxidized sucrose, central composite design, wound dressing

Abbreviations

ANOVA	Analysis of Variance
FTIR	Fourier Transform Infrared Spectroscopy
^{1}H NMR	proton nuclear magnetic resonance
WVTR	water vapor transmission rate
CCD	central composite design
H_0	null hypothesis
H_1	alternative hypothesis
μ	mean for the population
μ_0	hypothetical population mean
Df	degree of freedom
SS	sum of a square
MS	mean square
R^2	coefficient of determination
d	desirability
CV	coefficient of variation
OS	oxidized sucrose
OSH	oxidized sucrose hydrogel

1 Introduction

Hydrogels are highly valuable materials in the medical field, finding applications in various semi-solid preparations such as gels, creams, ointments, and patches. They are characterized by their hydrophilic and insoluble properties, which make them ideal for a wide range of applications [1]. They are soft materials with a three-dimensional crosslinked polymer network capable of holding significant amounts of water [2,3]. This high water content is due to the abundance of hydrophilic groups in the polymer network, which include –OH, –COOH, –$CONH_2$, –CONH, and –SO_2H [4,5]. These hydrophilic groups enable hydrogels to absorb and retain water, causing them to swell

* **Corresponding author: Chandra Wahyu Purnomo**, Chemical Engineering Department, Faculty of Engineering, Universitas Gadjah Mada, Jl. Grafika No. 2, Kampus UGM, Yogyakarta 55281, Indonesia, e-mail: chandra.purnomo@ugm.ac.id
Fitri Nur Kayati: National Research and Innovation Agency (BRIN), Jl. MH Thamrin No. 8, Jakarta 10340, Indonesia; Chemical Engineering Department, Faculty of Engineering, Universitas Gadjah Mada, Jl. Grafika No. 2, Kampus UGM, Yogyakarta 55281, Indonesia
Yuni Kusumastuti, Rochmadi: Chemical Engineering Department, Faculty of Engineering, Universitas Gadjah Mada, Jl. Grafika No. 2, Kampus UGM, Yogyakarta 55281, Indonesia

while maintaining their structure. Their insolubility is attributed to the three-dimensional network, allowing hydrogels to keep their shape [6]. The ability of hydrogels to absorb and retain water within the gel matrix gives them strong, flexible, and low interfacial pressure properties. Besides, they can provide regulated release of compounds and maintain a moist environment, so hydrogels are useful for a variety of applications, such as wound dressings [7,8], tissue engineering [9,10], biosensors [11,12], and drug delivery [13]. In terms of wound dressings, hydrogels could establish a physical barrier, remove extra exudate, enclose bioactive molecules, and provide a moist environment [8]. They also, in tissue engineering, offer the necessary biological and structural properties for the wounded area to successfully regenerate during the wound healing process [10,13].

There are no universally established standards for ideal wound dressings, but they should possess important features such as sufficient mechanical strength, the ability to absorb exudates, infection prevention, controlled drug release, ease of sterilization, and compatibility with the human body [14,15]. Previously, thin layer hydrogels with a thickness of 3 mm with characteristics such as transparency, high water content (greater than 90%), controlled drug release, adequate strength, and sterilizability were successfully synthesized for use in wound dressings using polyvinyl pyrrolidone with radiation methods [16]. Moreover, there have been developments in starch-based wound dressings with moderate mechanical strength, surpassing the strength of human skin (11.5 MPa) [17]. For instance, the mechanical properties of PVA/Starch/Essential Oils hydrogel membranes vary from 14 to 19 MPa depending on the type and amount of added essential oils [18]. Likewise, the mechanical properties of rice starch/chitosan composite films vary from 27 to 35 MPa based on the weight ratio of these two polymers [19].

Cassava starch is abundant, diverse, and vastly available, making it a promising candidate for various applications, including the fields of food, medicine, and environmental field [20–22]. However, its gel has suffered from low strength and stability [23–26]. To be used as a hydrogel for wound dressings, the properties of cassava hydrogel need improvement. In this study, a chemical treatment method involving crosslinking will be employed to enhance the characteristics of cassava starch gel. Crosslinking involves creating chemical bonds between hydroxyl groups (–OH) of starch molecules. Chemicals commonly used for crosslinking with starch include aldehydes like glutaraldehyde and formaldehyde [27]. However, due to their environmental toxicity, these chemicals are unsuitable for wound dressing products [28]. Based on previous research, oxidized sucrose has been considered an alternative, non-toxic crosslinking agent for starch [29,30]. This compound is produced by oxidizing sucrose into polar aldehydes, which have low toxicity and sufficient reactivity. Corn starch films crosslinked with oxidized sucrose achieved a tensile strength of 23 MPa and an elongation of 60% [29].

This study focused on optimizing the mechanical properties of cassava starch hydrogel through an improved crosslinking method [29–31]. The improvement was achieved by subjecting the gel to heat treatment using an autoclave after the gelatinization step. Such a treatment was necessary because cassava starch has higher viscosity during gelatinization compared to other starch types [24,25]. Further heating would help liquefy the cassava starch gel, making it more pourable during film casting. The improvement in film tensile strength was attainable by varying the composition of the crosslinking agent and plasticizer, referring to the central composite design (CCD) method, with two variables: oxidized sucrose and glycerol concentration. The resulting hydrogel products were then analyzed for tensile strength, morphology, and functional properties, such as swelling, water vapor transmission rate (WVTR), contact angle, and cytotoxicity.

2 Materials and methods

2.1 Materials

The primary raw material in this study was cassava starch, which had an amylose content of 21.17%, moisture content of 12.08%, and ash content of 0.11%. This cassava starch was sourced from one of the starch extraction industries in Lampung Province, Indonesia. Other materials, such as the components of the crosslinking agent and plasticizer, were purchased from Merck. These materials included sucrose, barium dichloride, sodium meta periodate (>98%), glycerol (99.7%), sodium hydroxide (NaOH), and hydrochloric acid (37%).

2.2 Preparation and hydrogel synthesis

The preparation of the hydrogel began with the preparation of the crosslinking agent, oxidized sucrose, followed by the production of the hydrogel using the crosslinking reaction between the starch and the crosslinking agent. The preparation of oxidized sucrose followed the method described by Xu [29]. 6.6 g of sucrose and 12.9 g of sodium meta periodate were dissolved in 200 mL of distilled water and stirred for 24 h. Subsequently, 7.0 g of barium dichloride

was added while stirring at 5°C for 1 h. The liquid and precipitate formed were separated using a centrifuge at 3,000 rpm for 20 min. The filtrate containing a polyaldehyde derivative of sucrose was stored at 5°C and was ready to be used as the crosslinking agent.

For synthesizing the hydrogel, 7.5 g of cassava starch was dissolved in 45 mL of distilled water and stirred with a magnetic stirrer. Specific ratios of oxidized sucrose and glycerol were then added according to the experimental design shown in Table 1. The solution was heated to 90°C for 30 min. The crosslinking process was further enhanced by heating the solution using an autoclave at 105°C for 10 min. The solution became more fluid and was easy to pour into the mold while still warm (>60°C). The solution in the mold was left to stand for 2 × 24 h at room temperature until it solidified into a gel. Subsequently, the gel was dried in an oven at 46°C to obtain dry hydrogel sheets for mechanical characterization.

2.3 Statistical analysis

To analyze the effect of the addition of oxidized sucrose and glycerol on tensile strength, a CCD was utilized, consisting of 13 trials and three replicates at the central point (Table 1). The results underwent regression analysis to evaluate the impact of treatments and variables, along with their respective interactions. Multiple linear regression and a second-order polynomial model were employed to estimate the regression coefficients based on the experimental data. The regression coefficients of the quadratic model were then tested, and the model was selected if it showed significance ($p < 0.05$), a lack of adjustment that was non-significant ($p > 0.05$), and suitability for explaining the phenomenon. All analyses were conducted using Minitab 16 software.

2.4 Hydrogel film characterization

The mechanical properties were analyzed following the modified ASTM D638-14 Standard Test Method for Plastic Tensile Properties. The sample was cut into sizes of 100 mm × 25.4 mm. The samples were tested using Labthink's XLW (E.C.) Auto Tensile Tester (Jinan, PR China) with a grip distance of 50 mm and a test speed set at 1 mm·min^{-1}. Three replications were conducted for each film-forming formula. Before testing, all samples were conditioned at 23°C for 48 h. Then, the strength of the best hydrogel film was comprehensively characterized, including morphological analysis, Fourier Transform Infrared Spectroscopy (FTIR), NMR, and other functional properties such as swelling, WVTR, contact angle, and cytotoxicity.

Morphological analysis was conducted using the VHX-5000 digital microscope, featuring magnification capabilities ranging from 0.1× to 5,000×. The microscope also facilitated the measurement of the contact angle of water droplets (0.1 microns) on the hydrogel's surface. ATR-FTIR Cary 630 (Agilent Technologies) was employed with the following settings: 5 Hz, four resolutions, 32 background scans, and 64 sample scans. The spectrum was collected in the mid-infrared range spanning 650 to 4,000 cm^{-1} wavenumbers. Data from each sample were gathered from three sample points.

NMR analysis was carried out to delineate the structural distinctions among oxidized sucrose, the crosslinked hydrogel, and cassava starch. The sample was characterized using an H NMR Bruker Avance III Spectrometer, operating at 400 MHz and a temperature of 70°C (512 scans). Dimethyl sulfoxide (DMSO) was used as the sample solvent.

The WVTR of the hydrogels was determined following the ASTM E96 Standard using a W3/031 WVTR Tester, Labthink-China. This instrument employs the cup method and is professionally designed for conducting WVTR tests on film specimens. To conduct the test, the hydrogels were cut into 33 cm^2 × 3 circles and sealed onto an aluminum permeation cup filled with water using silicone grease. A ring was used to secure the hydrogels in place. At a specific test temperature, a constant humidity difference was established between the two sides of the test specimen. Water vapor permeated through the sample and into the dry side. WVTR and other parameters were determined by measuring the weight changes of the test dish at various intervals. It is important to note that due to operational constraints of the equipment, this WVTR analysis was limited to six weighing cycles.

The gravimetric method was employed to analyze the swelling of the hydrogels in water. At room temperature, a predetermined amount of hydrogel film was immersed in water. The water absorbed by the hydrogel film was measured at specific intervals using an analytical balance until

Table 1: Matrix of experimental levels using a CCD

Factor/variable	−1 (Low)	0	+1 (High)
Oxidized sucrose (mL·g^{-1} of starch)	0.667	1.000	1.333
Gliserol (g·g^{-1} of starch)	0.053	0.067	0.080

it reached equilibrium. Eq. 1 was used to calculate the degree of swelling of the hydrogel.

$$\text{Degree of swelling (\%)} = \frac{m - m_0}{m_0} \times 100\% \quad (1)$$

where m_0 is the hydrogel mass at time 0 and m is the swollen hydrogel at time t.

Cytotoxicity testing was conducted using the MTT method. The sample pieces were dissolved in DMSO at a specific concentration (200 μg·mL^{-1}). The sample solution was subsequently diluted into six–nine different concentration levels and incubated for 24 h at 37°C. After incubation, the sample solution was filtered to remove any potential solid particles. Cell cultures were prepared in DMEM supplemented with 10% (v/v) fetal bovine serum (FBS) and seeded into 96-well microplates. The plates were then incubated for 24 h at 37°C in a humidified atmosphere with 5% CO_2. Following this, the diluted sample pieces were added to each well (100 μL per well for each concentration in triplicate), with wells containing only cell culture medium serving as controls. After an additional 24 h of incubation, the cell culture was treated with MTT. Diluted MTT reagent (1 mg·mL^{-1} in medium) was added to each well (100 μL) and incubated for 4 h in the incubator. After incubation, 100 μL of 10% SDS was added to each well, and the plates were left to shake at room temperature overnight. The optical density (OD) was subsequently measured using an ELISA Reader at a wavelength of 570 nm. Cytotoxicity for all concentration variations of the sample was assessed in a minimum of three separate experiments.

3 Results and discussion

The hydrogel, created by chemically linking cassava starch with oxidized sucrose and glycerol, maintains its structural coherence and exhibits attributes like transparency, homogeneity, and flexibility, as demonstrated in Figure 1. These attributes render it highly suitable for thorough analysis and examination of its film properties.

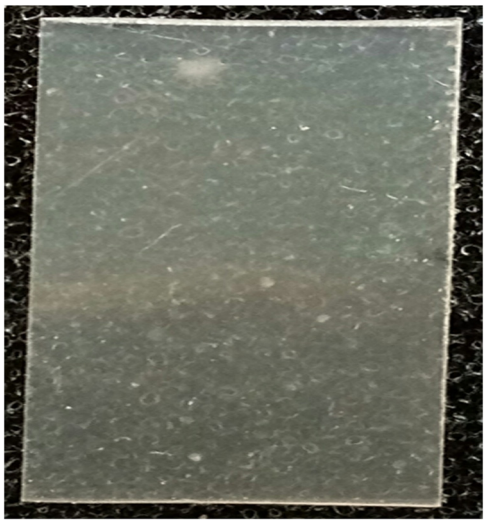

Figure 1: The hydrogel from the crosslinking of cassava starch with oxidized sucrose.

3.1 Optimization of hydrogel strength

The attempt to improve the mechanical strength of the hydrogel film included adjusting the crosslinking agent and plasticizer composition while maintaining a constant cassava starch content. A statistical approach utilizing experimental design was employed to reduce the number of required tests and circumvent the constraints of one-factor-at-a-time methods [32,33]. The results of the two-variable experimental design, which included three levels (−1, 0, +1) and consisted of 13 trials, along with the corresponding measurements of tensile strength, are summarized in Table 2. The highest tensile strength achieved in these experiments was 28.21 MPa.

The experimental results were then subjected to ANOVA, and the statistical significance of the model was evaluated using the *F*-test and *P*-test for ANOVA, as displayed in Table 3. The *F*-value of 245.89 signified the model's significance, while the Lack of Fit value of 4.370, which was smaller than the *F*-value, confirmed the model's importance in predicting tensile strength outcomes. The ANOVA results for the model revealed that both the linear model (p-value = 0.0) and the quadratic model (p-value = 0.0) were significant since their p-values were less than 0.05 (this study utilized a significance level of 5%). However, the non-linear model (p-value = 0.056), which involved interactions between factors, was not significant. The individual coefficient test values for the oxidized sucrose and glycerol composition both had p-values less than 0.05, indicating a significant influence on tensile strength. The Lack of Fit test results exhibited a p-value of 0.094, which exceeded 0.05, suggesting that the null hypothesis (H_0) was not rejected. This implied that there was no Lack of Fit, and the model employed in the experiment fit the data adequately.

The coefficient of determination R^2 assessed the model's goodness of fit, resulting in a value of 99.49% ($p < 0.05$), for the tensile strength of the hydrogel. This high R^2 value indicated that the model was highly effective in predicting the tensile strength of the hydrogel based on the predicted

Table 2: The experimental design for optimizing the composition of oxidized sucrose and glycerol

Std order	Run order	Pt type	Blocks	Oxidized sucrose (mL·g^{-1} of starch)	Glycerol (g·g^{-1} of starch)	Tensile strength (MPa)
1	12	1	1	0.667	0.053	18.7426
2	4	1	1	1.333	0.053	16.1465
3	6	1	1	0.667	0.080	12.3524
4	5	1	1	1.333	0.080	13.0055
5	1	−1	1	0.529	0.067	11.9713
6	2	−1	1	1.471	0.067	8.8552
7	13	−1	1	1.000	0.048	23.8595
8	10	−1	1	1.000	0.086	18.7497
9	11	0	1	1.000	0.067	27.9162
10	7	0	1	1.000	0.067	27.0229
11	3	0	1	1.000	0.067	27.4644
12	9	0	1	1.000	0.067	28.2137
13	8	0	1	1.000	0.067	27.5670

values generated by the CCD model. The mathematical model representing the impact of the factors (oxidized sucrose/OS and glycerol) on the response (tensile strength) can be expressed by the following equation:

$$\begin{aligned}\text{Tensile} = {} & -110.76 + (144.034 * \text{OS}) \\ & + (2,184.20 * \text{Glycerol}) - (79.30 * \text{OS} * \text{OS}) \\ & -(18,930.50 * \text{Glycerol} * \text{Glycerol}) \\ & + (182.766 * \text{OS} * \text{Glycerol})\end{aligned} \quad (2)$$

The results of the model for the response are visually represented through two-dimensional (2D) contour plots and surface plots in Figures 2 and 3, respectively. The surface plot (Figure 2) shows the relationship between the percentage of oxidized sucrose and glycerol, forming a distinctive peak optimization pattern. As the ratio of oxidized sucrose and glycerol decreases, the tensile strength value tends to increase. However, there is a certain point at which a further decrease in tensile strength occurs when the addition of oxidized sucrose and glycerol reaches the optimum level.

Conversely, the contour plot (Figure 3) illustrates combinations of the two factors with varying proportions that yield the same tensile strength response. The plots in both Figures 2 and 3 suggest the presence of stationary points, indicating that the optimal tensile strength response is achieved through a balanced combination of both factors.

The desirability function is employed to optimize the response in order to reach the target value. This optimization is carried out by converting the response into a desired value, denoted as "d" (desirability), where $0 \le d \le 1$. The lower limit for optimizing the response is set

Table 3: ANOVA for tensile strength (MPa) with two factors

Source	DF	Seq SS	Adj SS	Adj MS	*F*	*P*
Regression	5	617.612	617.612	123.522	245.890	0.000
Linear	2	40.142	40.142	20.071	39.950	0.000
Oxidized sucrose	1	5.040	5.040	5.040	10.030	0.016
Glycerol	1	35.102	35.102	35.102	69.880	0.000
Square oxidized	2	574.831	574.831	287.415	572.150	0.000
Sucrose * oxidized Sucrose	1	496.041	540.074	540.074	1,075.110	0.000
Glycerol * Glycerol	1	78.790	78.790	78.790	156.850	0.000
Interaction	1	2.639	2.639	2.639	5.250	0.056
Oxidized Sucrose * glycerol	1	2.639	2.639	2.639	5.250	0.056
Residual error	7	3.516	3.516	0.502		
Lack-of-fit	3	2.694	2.694	0.898	4.370	0.094
Pure error	4	0.822	0.822	0.206		
Total	12	621.128				

DF, degree of freedom; SS, sum of a square; MS, mean square.
S = 0.708760; R^2 = 99.43%; $R^2_{(adj)}$ = 99.03%; F = MS(factor)/MS(error).

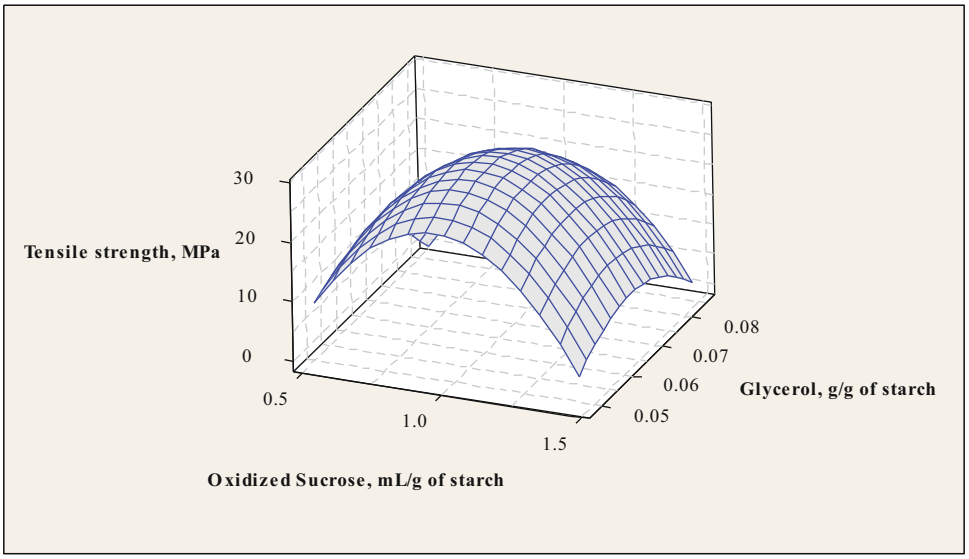

Figure 2: Surface plot curve of tensile strength optimization.

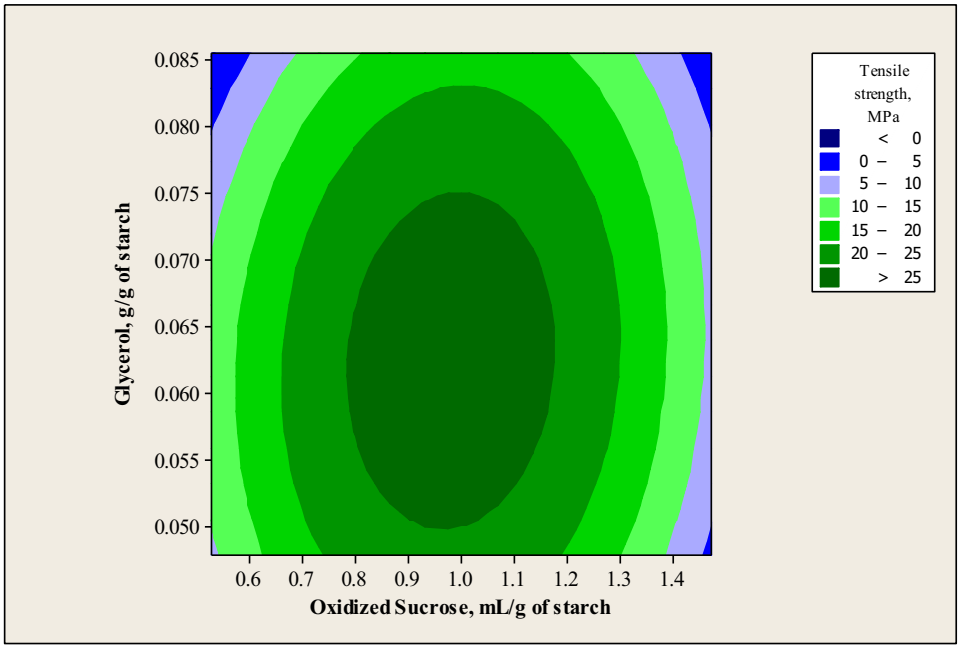

Figure 3: Counter plot curve of tensile strength optimization.

at 10, while the upper limit is determined to be 28, with both the weight and importance level of the response assigned a value of one. The results of the optimization calculation using the desirability function are presented in Table 4.

The visualization graph of the optimization process using the desirability function to achieve a tensile strength response of 27.9928 is depicted in Figure 4. This chart illustrates that the desirability value (*d*) reaches its maximum when the factor values align with the red-colored line. This occurs when the amount of oxidized sucrose is 0.9762 $mL \cdot g^{-1}$ of starch, and glycerol is 0.0624 $g \cdot g^{-1}$ of starch. Within the desirability graph (Figure 4), a black curve line represents the value of d for each response, while the blue dashed line indicates the response value at the optimal point, which is 27.9928 MPa. This optimal point is achieved when the *d* value reaches 0.999601. The graph effectively demonstrates the optimized conditions (maximum desirability) for attaining the

Table 4: Desirability function of tensile strength optimization

Factor		Response (tensile strength, MPa)	Desirability
Oxidized sucrose (mL·g^{-1} of starch)	0.9762	27.9928	0.999601
Gliserol (g·g^{-1} of starch)	0.0624		

desired tensile strength response of 27.9928 MPa by adjusting the proportions of oxidized sucrose and glycerol.

Following the attainment of the optimal response value and the assessment of the analysis results' accuracy, a confirmation experiment was carried out. This experiment involved replicating the process three times at the factor levels corresponding to the optimal response value. The data from the confirmation experiment were then subjected to a one-sample *t*-test to compare the average values of the confirmation experiment with the estimated value for the response.

In this one-sample *t*-test, two hypotheses were considered: the null hypothesis (H_0) and the alternative hypothesis (H_1) with $\mu_0 = 27.9928$ for the tensile strength response, and the significance level was set at $\alpha = 0.05$. The null hypothesis (H_0) posits that the population mean (μ) is equal to the hypothetical population mean: $\mu = \mu_0$, while the alternative hypothesis (H_1) suggests that the population mean differs from the hypothetical population mean: $\mu \neq \mu_0$.

The results of the one-sample *t*-test for the confirmation experiment data are presented in Table 5. These results indicate that the *p*-value for the tensile strength response is greater than 0.05, implying that H_0 was accepted. Consequently, the values found in the confirmation experiment concerning the oxidized sucrose and glycerol composition response were in agreement with the estimated values. Additionally, the evaluation of the coefficient of variation (CV) value indicates a 3% (or <5%), signifying good stability in the confirmed test results.

The outcomes of the optimization for tensile strength were subsequently compared with previous research that also utilized starch with the cross-linking agent, oxidized sucrose. As indicated in Table 6, the utilization of oxidized sucrose as a starch cross-linking agent yielded varying tensile strength values. This variance could be attributed to differences in the cross-linking reaction process between starch and oxidized sucrose, including variations in methods (temperature treatment) and reagent compositions. For instance, a high-temperature treatment with a curing process led to an increase in tensile strength up to 23 MPa and a strain of 60%, results that closely resembled this study, which employed temperature treatment with an autoclave process and optimized the composition of cross-linking agents and plasticizers. In contrast, the addition of cellulose nanofibrils produced only a marginal increase in

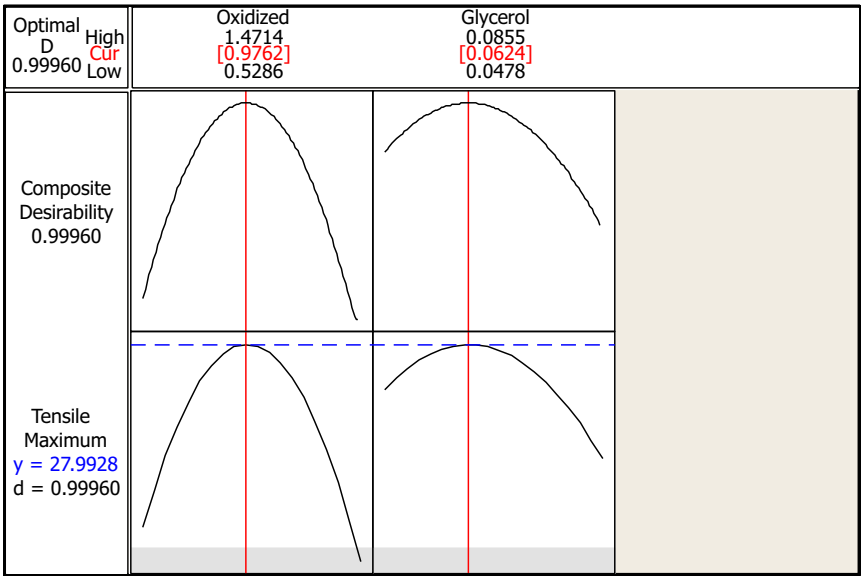

Figure 4: Desirability curve of tensile strength optimization.

Table 5: The results of the one-sample *t*-test for the confirmation experiment data

The confirmation experiment data	Value
Tensile strength experiment 1	26.75
	27.37
	27.13
Tensile strength experiment 2	29.37
	28.22
	27.34
Tensile strength experiment 3	27.82
	26.77
	27.21
The estimated values	27.9928
Mean sample	27.552
p-Value	0.151
% CV	3.00

tensile strength, with the value remaining significantly lower than the results achieved in this research. The enhanced mechanical properties can be attributed to the abundance of aldehyde groups in oxidized sucrose, which facilitated more effective reactions with starch hydroxyl groups.

3.2 Hydrogel characterization

Examining the characterization of the hydrogel at the point of optimal tensile strength is essential to reinforce the assessment of the hydrogel product's appropriateness as a framework for wound dressing. This examination encompasses aspects such as morphology, FTIR , ^{1}H NMR (Proton Nuclear Magnetic Resonance), as well as other functional properties, including swelling, WVTR, contact angle, and cytotoxicity.

Table 6: Comparison of tensile properties of starch crosslinked with oxidized sucrose

Crosslinking agent	Tensile strength (MPa)	Tensile strain (%)	Ref
Oxidized sucrose	27	70	This work
Oxidized sucrose	23	60	[29]
Oxidized sucrose	3	33	[31]
Oxidized sucrose + cellulose nanofibril	5	40	[31]

3.2.1 Morphology

A digital microscope was employed to examine the surface morphology of both the dried hydrogel and the hydrogel after swelling in water, as depicted in Figure 5. The analysis revealed that neither of the samples displayed any cavities or interruptions at the boundary between the hydrogel matrix and the water (as the filler), signifying strong adhesion within the hydrogel structure [34]. The appearance of the swollen hydrogel surface aligns with the formation of a dense structure in the crosslinked sample, demonstrating an effective blockage of hydrophilic hydroxyl groups. This phenomenon can impede the ingress of water vapor and oxygen, consequently reducing the transmission rate.

3.2.2 FTIR

FTIR spectroscopy was utilized to examine the spectral changes in starch before and after crosslinking with oxidized sucrose. The reaction involved the aldehyde group (–C = O) in oxidized sucrose and the hydroxyl group (–OH)

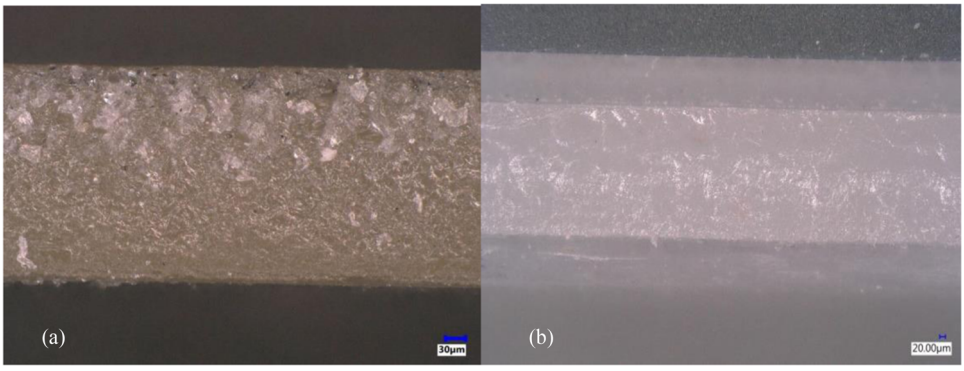

Figure 5: Digital microscope images of the cross-sectional sides of the surfaces of (a) dry hydrogel and (b) water-swelled hydrogel.

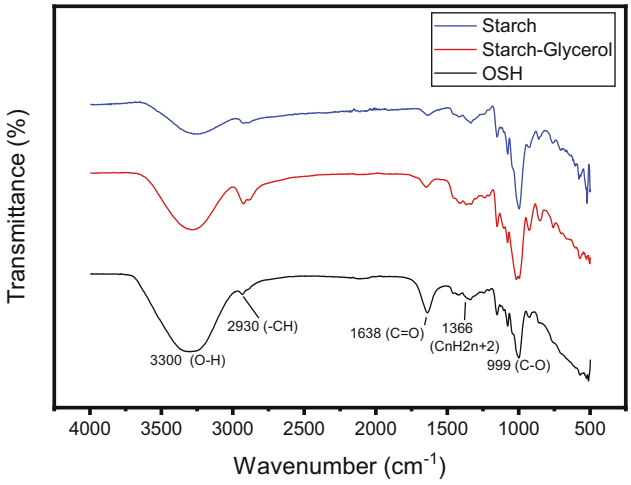

Figure 6: FTIR spectroscopy of cassava starch, cassava starch-glycerol, cassava starch-oxidized sucrose hydrogel (OSH).

in starch, resulting in the formation of an ether bond (–C–O–C–). As shown in Figure 6, the FTIR spectrum of starch crosslinked with oxidized sucrose (OSH) displayed more pronounced and broader characteristic peaks in the range of 3,200–3,500 cm^{-1} when compared to pure starch and glycerol starch. This indicates a robust interaction between the hydroxyl groups of starch and the aldehyde group of oxidized sucrose, leading to a reduction in hydroxyl groups as they underwent conversion into ethers [31,35]. The absorption peak around 2,930 cm^{-1} indicates the asymmetric stretching vibration of carbon–hydrogen ($–CH_2$). However, the new peak indicating the stretching vibration of C–O–C was not observed as mentioned in previous references, which typically appears around 1,319 cm^{-1} [30]. This area may overlap with a more significant peak around 1,638 cm^{-1}, corresponding to C═O bonding [31].

3.2.3 ^{1}H NMR

The results of the ^{1}H NMR spectra analysis for cassava starch can be seen in Figure 7(a), while those of cassava starch crosslinked with oxidized sucrose can be seen in Figure 7(b). In both spectra, the prominent first and second peaks around δ 2.5 and 3.5 ppm indicate the presence of DMSO and water, which are the solvents used in the solvent medium [30,36]. The six peaks observed in the ^{1}H NMR spectrum of cassava starch correspond to the positions of hydroxyl protons that are linked to six carbons in the glucose units of starch [37].

The ^{1}H NMR spectrum of the OSH in Figure 7(b) displays a split peak at δ 4.6 ppm, which is a result of the crosslinking process. This separation in the ^{1}H NMR spectrum is due to changes in the proton environment [29]. The peak separation in the crosslinked starch is attributed to the formation of acetal bonds resulting from the reaction between the C6 of starch and the aldehyde groups of oxidized sucrose [30]. These peaks provide confirmation of the formation of ether bonds in the crosslinking reaction between the aldehyde groups of oxidized sucrose and the hydroxyl groups of starch and glycerol, as illustrated in the predicted reaction mechanism in Figure 8.

3.2.4 Swelling

Swelling characterization was performed on samples that exhibited optimal tensile strength. Figure 9 illustrates the hydrogel both before and after the swelling process. During the swelling process, the hydrogel absorbs water, leading to changes in its size.

Significant swelling was evident within the initial 1–5 h, followed by a gradual increase in swelling that tended to stabilize after being left for up to 48 h. This reached its maximum swelling capacity at 95%, as illustrated in Figure 9. The hydrogel maintained its structural integrity throughout the soaking period and did not disintegrate. This property is anticipated to be beneficial for using the hydrogel as a wound dressing medium. It effectively collects wound exudates in gel form, providing a wound-suppressing and preserving effect while also reducing the unpleasant odor produced by the exudates at the wound site, thereby preventing bacterial infections [38] and mitigating the malodorous effects [18].

3.2.5 WVTR

Wound dressings play a crucial role in managing water loss, as they help maintain an optimal level of moisture on the wound surface, creating a favorable environment for natural healing [39]. In light of this, the study assessed the WVTR of the hydrogel product with optimal tensile strength. Evaluating WVTR offers insights into the passage of water vapor from the wound bed, through the dressing, to the surrounding environment over a specified time frame, typically measured in units of g per m^2 per 24 h [39–41]. Different types of wound dressings have varying WVTR values depending on their material composition [41]. For instance, porous gauze dressings have a WVTR value of approximately 1,600 g per m^2 per 24 h, while occlusive dressings like hydrocolloids have a WVTR value of <300 g per m^2 per 24 h [41]. However, wound dressings can be considered suitable moisture barriers (occlusive)

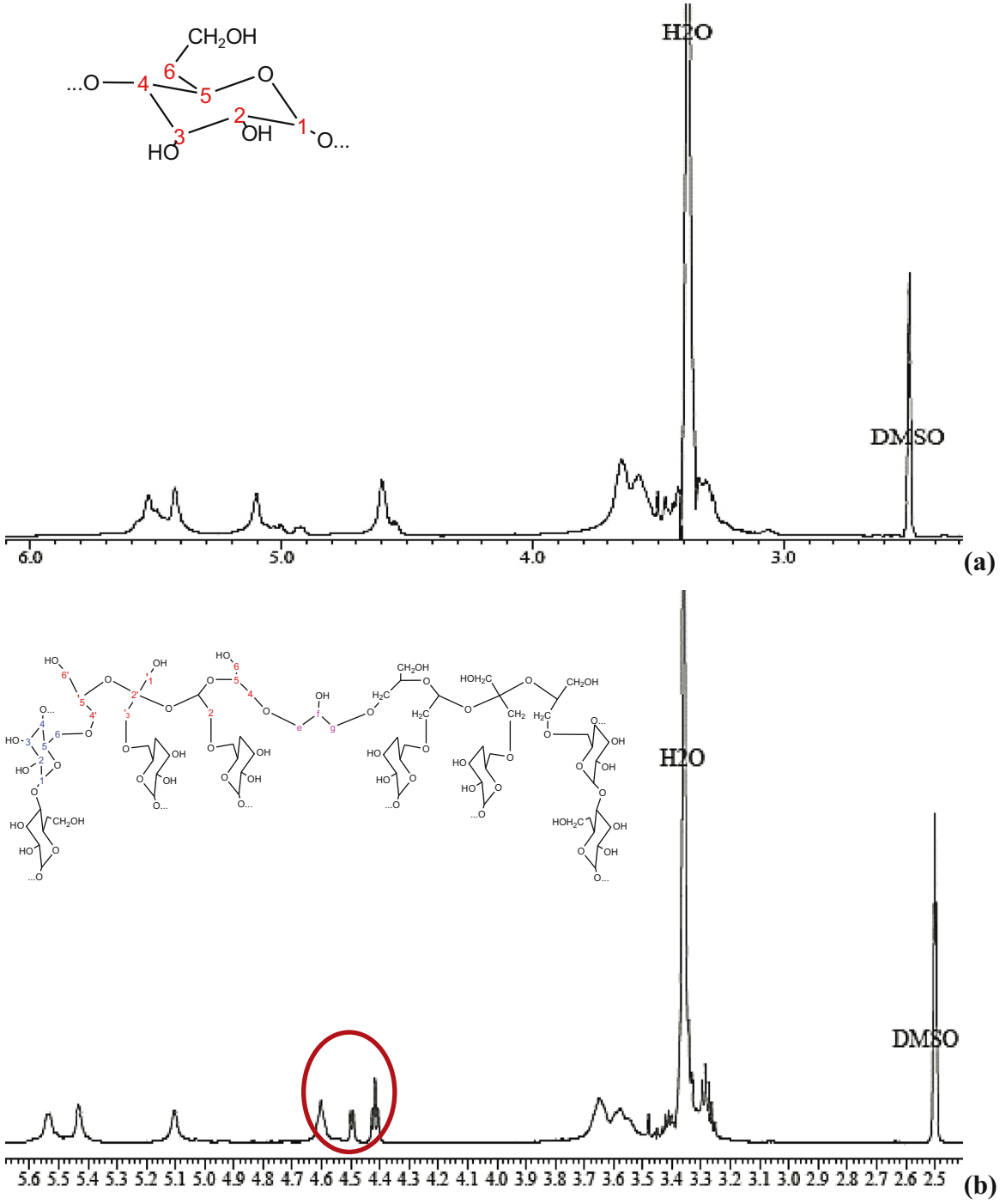

Figure 7: The ^{1}H NMR spectra of (a) cassava starch and (b) OSH.

if their moisture retention level is <840 g per m^2 per 24 h [40]. If the WVTR value is excessively high, it can result in wound dehydration, whereas an excessively low WVTR may lead to the accumulation of wound exudate [39]. The evaluation results show that the WVTR value of the hydrogel product in this study was 714.92 g per m^2 per 24 h, as seen in Figure 10. Therefore, the hydrogel produced in this study could be considered an effective wound dressing that serves as a reliable moisture barrier, facilitating an optimal healing environment.

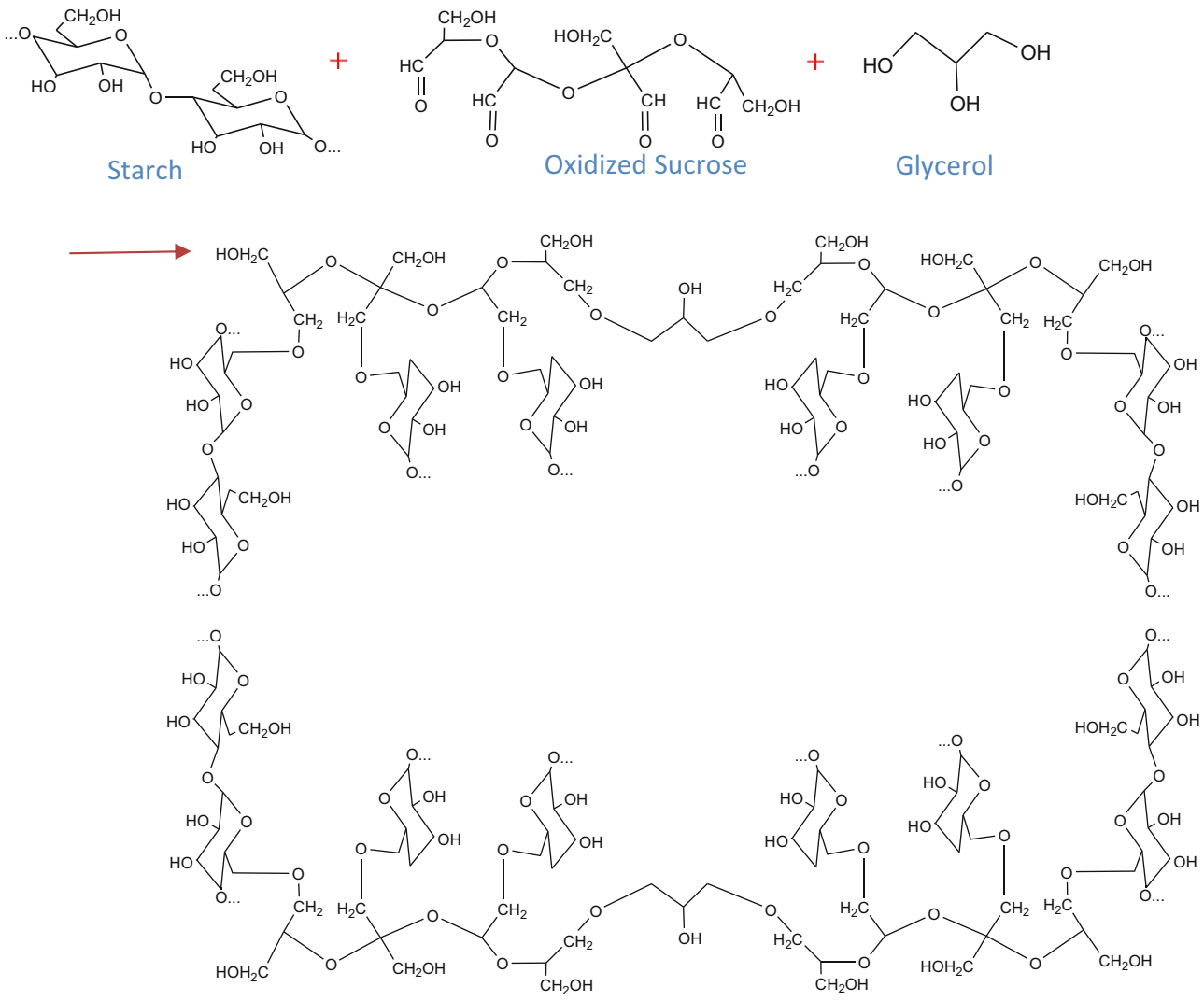

Figure 8: Prediction of the reaction mechanism for cassava starch and oxidized sucrose crosslinking.

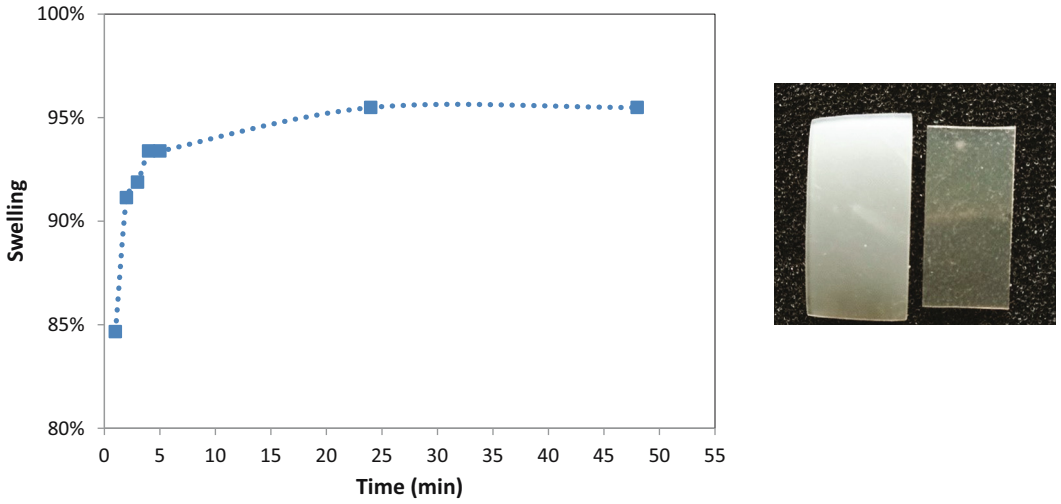

Figure 9: Swelling process of hydrogel with observation for 48 h.

3.2.6 Contact angle

The hydrophobicity of the hydrogel product in this study was assessed by measuring the water contact angle. Starch, as the primary raw material, tends to have low moisture resistance due to its hydrophilic nature [42]. However, the crosslinking between the hydroxyl groups of starch and the aldehyde groups of oxidized sucrose substantially reduced the hydrophilic hydroxyl groups, resulting in an increased hydrophobicity of the hydrogel surface [31]. Changes in the water contact angle of the hydrogel were monitored at 1-min intervals, as illustrated in both Figures 11 and 12.

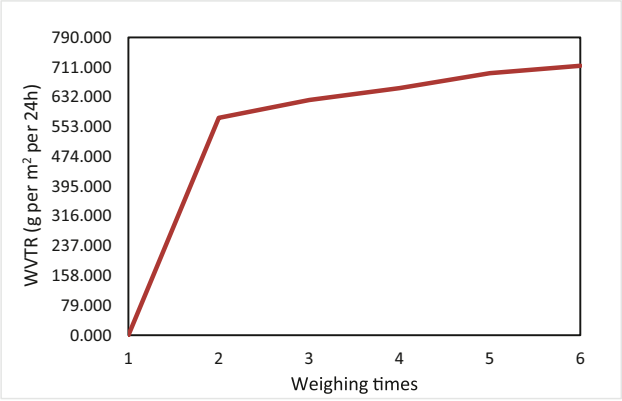

Figure 10: Results of WVTR test for the hydrogel.

Based on the observations, the initial water contact angle of the hydrogel was measured at 74.76° at 0 min, and it decreased over time, as depicted in Figure 12. In general, a surface with a water contact angle of less than 90° is considered hydrophilic, while a surface with a water contact angle greater than 90° is considered hydrophobic [43]. Hydrophilic surfaces attract liquids strongly and completely wet the surface over time, resulting in the contact angle approaching 0°. According to Giridhar et al. [44], surface wetting can be categorized as hydrophobic (contact angle >80°), moderately wettable (contact angle 48–62°), and hydrophilic (contact angle < 35°). A contact angle in the range of 40–70° is typically considered moderately hydrophilic [45], which is ideal for promoting cell adhesion

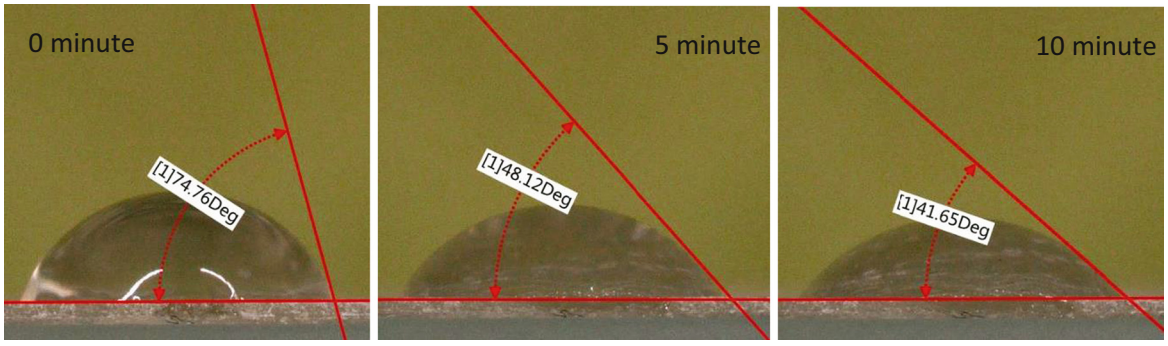

Figure 11: Images of the same sessile drop of the hydrogel at different time intervals.

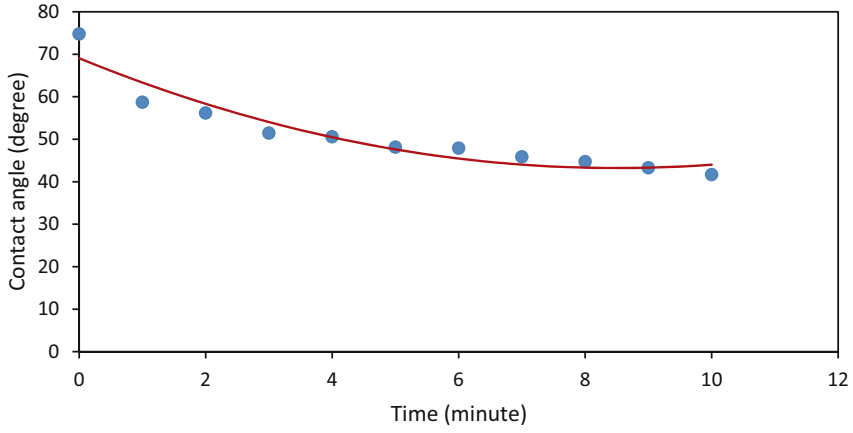

Figure 12: The water contact angle of hydrogel changes as a function of time.

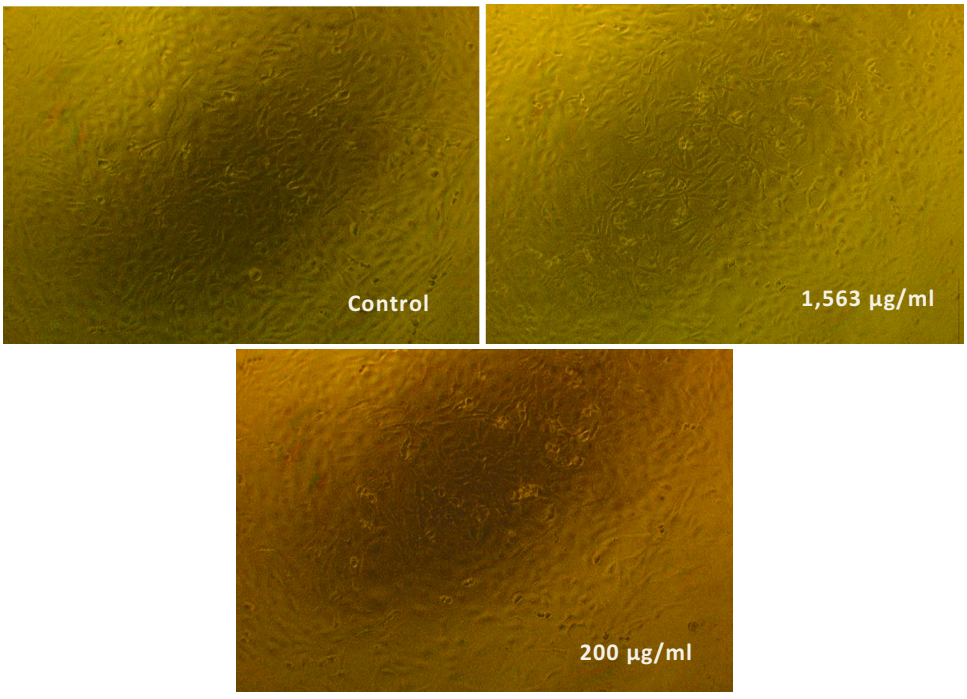

Figure 13: *In vitro* cytotoxicity test of hydrogel using NIH3T3 cells for a 24-h contact.

and wound-healing processes. The hydrogel surface in this study falls within this moderately wettable range, with a contact angle value of 74.76°, making it suitable for supporting cell adhesion during the wound-healing process.

3.2.7 Cytotoxicity

Biodegradable polymers intended for medical use must primarily demonstrate biocompatibility in specific environments [46]. In this context, the first essential assessment of biocompatibility for the hydrogel created in this study involves *in vitro* cytotoxicity testing. Even though the fundamental raw materials used in this hydrogel, namely starch and oxidized sucrose, are recognized as non-toxic substances [47–50], conducting this testing remains imperative. The key objective is to verify that the crosslinked reaction products of these materials do not exert any harmful effects on cells when applied as wound dressings.

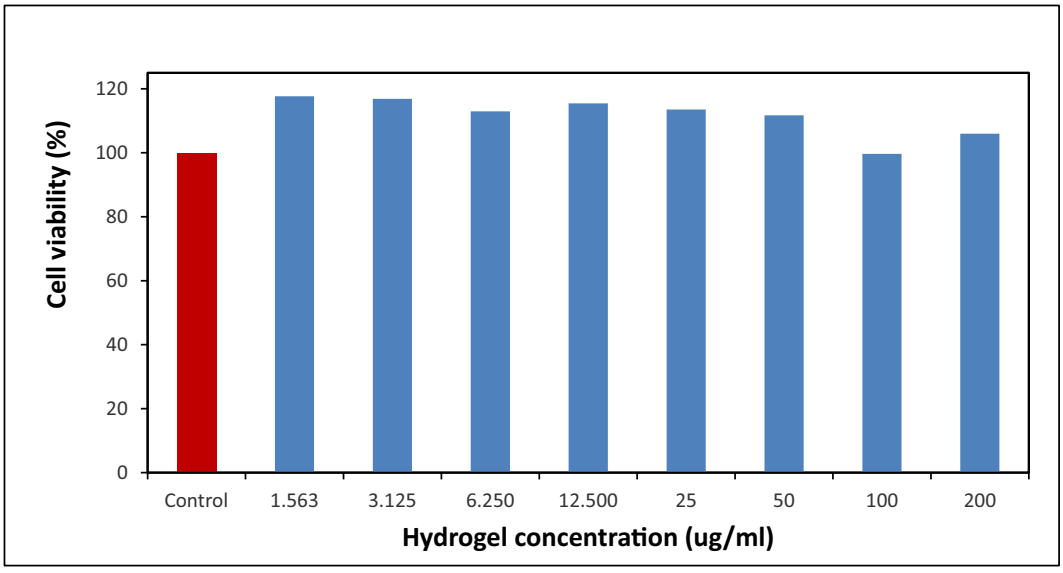

Figure 14: MTT Assay of NIH3T3 cells with variations of hydrogel concentration.

To ensure uniformity in the test samples with the cell medium, the hydrogel was dissolved in DMSO. The dissolution process was tested at various concentrations, reaching the maximum saturation level of the hydrogel in DMSO. When saturated, the hydrogel becomes challenging to dissolve uniformly in DMSO. In this study, concentration variations of the hydrogel in DMSO were examined within the range of 1.563–200 $\mu g \cdot mL^{-1}$, with cell observations made after 24 h. The direct *in vitro* contact test results, using NIH3T3 cells (a mouse fibroblast cell line), revealed that cells exposed to the lowest concentration (1.563 $\mu g \cdot mL^{-1}$) and the highest concentration (200 $\mu g \cdot mL^{-1}$) of the test samples maintained their typical elongated morphology, similar to the positive control. These cells exhibited no adverse responses, such as detachment or cell lysis, indicating the absence of toxic effects (Figure 13).

Moreover, the quantitative assessment of NIH3T3 fibroblast cell viability was conducted by measuring their metabolic activity using the MTT colorimetric assay. An increase in metabolic activity relative to the control indicates improved cell viability resulting from cell proliferation during the test period. In Figure 14, the results display the activity of NIH3T3 fibroblast cells when in contact with the hydrogel samples, and this activity decreased as the concentration of the hydrogel increased. Specifically, at a concentration of 1.563 $\mu g \cdot mL^{-1}$, the cell viability was measured at 117.66%, and at the highest concentration of 200 $\mu g \cdot mL^{-1}$, it was 105.97%. Despite the decrease in cell activity, these values still indicate no significant toxic effects on cell proliferation, aligning with the control test results when hydrogel samples were not used.

Certainly, the cytotoxicity testing conducted in this study serves as a valuable complement to the overall characterization of the hydrogel. Based on these results, the hydrogel can be deemed a suitable material for wound dressings. It has demonstrated strength, an effective swelling capacity for absorbing wound exudate, and safety when in contact with skin cells. These attributes collectively position the hydrogel as a promising candidate for wound dressing applications.

4 Conclusions

The development of a cassava-based hydrogel, incorporating oxidized sucrose as a crosslinking agent and glycerol as a plasticizer, has been successfully achieved. Tensile strength optimization was conducted using a CCD in Minitab 16 by varying the composition of oxidized sucrose and glycerol. ANOVA analysis revealed that both variables significantly impact tensile strength (p-value <0.05). The optimization process yielded an optimal tensile strength of 27 MPa, with the use of 0.9762 mL of oxidized sucrose per gram of starch and 0.0624 g of glycerol per gram of starch. Confirmation tests supported these values with a p-value exceeding 0.05, indicating the consistency of the estimations. Further characterization through FTIR and 1H NMR analyses confirmed the presence of crosslinking between the hydroxyl groups of starch and the aldehyde groups of oxidized sucrose. Functional characterization revealed that the hydrogel exhibited a swelling capacity of 95%, a WVTR of 714.92 g per m^2 per 24 h, a contact angle of 74.76°, and a cell viability value exceeding 100%. These results collectively demonstrate the hydrogel's potential for use in wound dressings. It possesses strong mechanical properties, the ability to absorb exudates, effective moisture retention, moderate wettability/hydrophilicity, and it does not exhibit significant toxicity toward cell proliferation, as indicated by cytotoxicity testing using NIH3T3 cells (a mouse fibroblast cell line).

Acknowledgements: The authors extend their sincere appreciation to the Directorate of Research and Community Service at Universitas Gadjah Mada for their financial support of this research project through Grant RTA 2021. Additionally, the authors are thankful for the support provided by the National Research and Innovation Agency (BRIN) for the use of laboratory facilities.

Funding information: The research was funded by the Directorate of Research and Community Service at Universitas Gadjah Mada.

Author contributions: Fitri Nur Kayati: Writing – original draft, conceptualization, methodology, investigation, and visualization; Chandra Wahyu Purnomo: writing – review, conceptualization, investigation, supervision, project administration, and funding acquisition; Yuni Kusumastuti: writing-review, investigation, and supervision; Rochmadi: writing-review, investigation, supervision writing-review, and conceptualization.

Conflict of interest: The authors state no conflict of interest.

Data availability statement: The data sets generated during and/or analyzed during the current study are available from the corresponding author on reasonable request.

References

[1] El Sayed MM. Production of polymer hydrogel composites and their applications. J Polym Environ. 2023;31(7):2855–79. doi: 10.1007/s10924-023-02796-z.

[2] Hua J, Björling M, Larsson R, Shi Y. Friction control of Chitosan-Ag hydrogel by silver ion. ES Mater Manuf. 2022;16:30–6.

[3] Cheng K, Zou L, Chang B, Liu X, Shi H, Li T, et al. Mechanically robust and conductive poly(acrylamide) nanocomposite hydrogel by the synergistic effect of vinyl hybrid silica nanoparticle and polypyrrole for human motion sensing. Adv Compos Hybrid Mater. 2022;5(4):2834–46. doi: 10.1007/s42114-022-00465-8.

[4] Kartika R, Gadri A, Darma GCE. Formulasi Basis Sediaan Pembalut Luka Hidrogel dengan Teknik Beku Leleh Menggunakan Polimer Kappa Karagenan. Pros Penelit Spes Unisba. 2015;1:643–8.

[5] Bajpai SK, Singh S. Analysis of swelling behavior of poly(methacrylamide-co-methacrylic acid) hydrogels and effect of synthesis conditions on water uptake. React Funct Polym. 2006;66(4):431–40.

[6] Swindle-Reilly KE, Reilly MA, Ravi N. 5 - Current concepts in the design of hydrogels as vitreous substitutes. In Woodhead Publishing Series in Biomaterials, Biomaterials and Regenerative Medicine in Ophthalmology. In Traian V, Chirila DGH, editors. 2nd edn. Sawston: Woodhead Publishing; 2016. p. 101–30. https://www.sciencedirect.com/science/article/pii/B9780081001479000055.

[7] Ode Boni BO, Lamboni L, Mao L, Bakadia BM, Shi Z, Yang G. *In vivo* performance of microstructured bacterial cellulose-silk sericin wound dressing: effects on fibrosis and scar formation. Eng Sci. 2022;19:175–85.

[8] Bakadia BM, Zhong A, Li X, Boni BOO, Ahmed AAQ, Souho T, et al. Biodegradable and injectable poly(vinyl alcohol) microspheres in silk sericin-based hydrogel for the controlled release of antimicrobials: application to deep full-thickness burn wound healing. Adv Compos Hybrid Mater. 2022;5(4):2847–72. doi: 10.1007/s42114-022-00467-6.

[9] Choi S, Raja IS, Selvaraj AR, Kang MS, Park TE, Kim KS, et al. Activated carbon nanofiber nanoparticles incorporated electrospun polycaprolactone scaffolds to promote fibroblast behaviors for application to skin tissue engineering. Adv Compos Hybrid Mater. 2023;6(1):1–14. doi: 10.1007/s42114-022-00608-x.

[10] Kuang T, Chen S, Gu Z, Shen Z, Hejna A, Saeb MR, et al. A facile approach to fabricate load-bearing porous polymer scaffolds for bone tissue engineering. Adv Compos Hybrid Mater. 2022;5(2):1376–84. doi: 10.1007/s42114-022-00418-1.

[11] Li T, Wei H, Zhang Y, Wan T, Cui D, Zhao S, et al. Sodium alginate reinforced polyacrylamide/xanthan gum double network ionic hydrogels for stress sensing and self-powered wearable device applications. Carbohydr Polym. 2023;309(Jan):120678. doi: 10.1016/j.carbpol.2023.120678.

[12] Kong D, El-Bahy ZM, Algadi H, Li T, El-Bahy SM, Nassan MA, et al. Highly sensitive strain sensors with wide operation range from strong MXene-composited polyvinyl alcohol/sodium carboxymethylcellulose double network hydrogel. Adv Compos Hybrid Mater. 2022;5(3):1976–87. doi: 10.1007/s42114-022-00531-1.

[13] Arun A, Malrautu P, Laha A, Ramakrishna S. Gelatin nanofibers in drug delivery systems and tissue engineering. Eng Sci. 2021;16:71–81.

[14] Mann A, Wound BJT. Healing studies and interfacial phenomena: use and relevance of the corneal model. In: Woodhead Publishing Series in Biomaterials, Advanced Wound Repair Therapies. Sawston: Woodhead Publishing; 2011. p. 284–320.

[15] Tighe BJ. Hydrogels. In: Encyclopedia of Advance Materials. United Kingdom: Elsevier Inc. Vol. 2; 1994. p. 1060.

[16] Rosiak JM, Janik I, Kadlubowski S, Kozicki M, Kujawa P, Stasica P. PU Radiation synthesis and modification of polymers for biomedical applications. Vienna: Int At Energy Agency. Vol. 1324; 2002. p. 5–47.

[17] Hassan A, Niazi MBK, Hussain A, Farrukh S, Ahmad T. Development of anti-bacterial PVA/Starch based hydrogel membrane for wound dressing. J Polym Environ. 2018;26(1):235–43.

[18] Altaf F, Niazi MBK, Jahan Z, Ahmad T, Akram MA, safdar A, et al. Synthesis and characterization of PVA/Starch hydrogel membranes incorporating essential oils aimed to be used in wound dressing applications. J Polym Environ. 2021;29(1):156–74. doi: 10.1007/s10924-020-01866-w.

[19] Bourtoom T, Chinnan MS. Preparation and properties of rice starch-chitosan blend biodegradable film. LWT - Food Sci Technol. 2008;41(9):1633–41.

[20] Xie X, Gao H, Luo X, Zhang Y, Qin Z, Ji H. Polyethyleneimine-modified magnetic starch microspheres for Cd(II) adsorption in aqueous solutions. Adv Compos Hybrid Mater. 2022;5(4):2772–86. doi: 10.1007/s42114-022-00422-5.

[21] Zhou D, Li D, Liu M, Zhong X, Wei H, Wang Z, et al. Experimental parameters affecting cross-linking density and free-thaw stability of cross-linked porous starch. ES Food Agrofor. 2021;5:20–8.

[22] Chen Y, Guo Z, Das R, Jiang Q. Starch-based carbon nanotubes and Graphene: preparation, properties and applications. ES Food Agrofor. 2020;2:13–21.

[23] Chinma CE, Ariahu CC, Abu JO. Chemical composition, functional and pasting properties of cassava starch and soy protein concentrate blends. J Food Sci Technol. 2013;50(6):1179–85.

[24] Mhaske P, Wang Z, Farahnaky A, Kasapis S, Majzoobi M. Green and clean modification of cassava starch–effects on composition, structure, properties and digestibility. Crit Rev Food Sci Nutr. 2022;62(28):7801–26. doi: 10.1080/10408398.2021.1919050.

[25] Wang Z, Mhaske P, Farahnaky A, Kasapis S, Majzoobi M. Cassava starch: Chemical modification and its impact on functional properties and digestibility, a review. Food Hydrocoll. 2022;129:129107542. doi: 10.1016/j.foodhyd.2022.107542.

[26] Huerta-Abrego A, Segura-Campos M, Chel-Guerrero L, Betancur-Ancona D. Changes in the functional properties of three starches by interaction with lima bean proteins. Food Technol Biotechnol. 2010;48(1):36–41.

[27] Kapelko M, Zięba T, Michalski A, Gryszkin A. Effect of cross-linking degree on selected properties of retrograded starch adipate. Food Chem. 2015;167:124–30.

[28] Xu H, Liu P, Mi X, Xu L, Yang Y. Potent and regularizable crosslinking of ultrafine fibrous protein scaffolds for tissue engineering using a cytocompatible disaccharide derivative. J Mater Chem B. 2015;3(32):3609.

[29] Xu H, Canisag H, Mu B, Yang Y. Robust and flexible films from 100% starch cross-linked by biobased disaccharide derivative. ACS Sustain Chem Eng. 2015;3:2631–9.

[30] Wang P, Sheng F, Tang SW, Chen L, Nawaz A, Hu C, et al. Synthesis and characterization of corn starch crosslinked with oxidized sucrose. Starch - Stärke. 2018;1800152:1–8.

[31] Balakrishnan P, Sreekala MS, Geethamma VG, Kalarikkal N, Kokol V, Volova T, et al. Physicochemical, mechanical, barrier and antibacterial properties of starch nanocomposites crosslinked with pre-oxidised sucrose. Ind Crops Prod. 2019;130:398–408.

[32] Md. Din MF, Ponraj M, Van Loosdrecht M, Ujang Z, Chelliapan S, Zambare V. Utilization of palm oil mill effluent for polyhydroxyalkanoate production and nutrient removal using statistical design. Int J Environ Sci Technol. 2014;11(3):671–84.
[33] Tripathi AD, Srivastava SK, Singh RP. Statistical optimization of physical process variables for bio-plastic (PHB) production by Alcaligenes sp. Biomass and Bioenergy. 2013;55:243–50. doi: 10.1016/j.biombioe.2013.02.017.
[34] Rico M, Rodríguez-Llamazares S, Barral L, Bouza R, Montero B. Processing and characterization of polyols plasticized-starch reinforced with microcrystalline cellulose. Carbohydr Polym. 2016;149:83–93. doi: 10.1016/j.carbpol.2016.04.087.
[35] Kumirska J, Czerwicka M, Kaczyński Z, Bychowska A, Brzozowski K, Thöming J, et al. Application of spectroscopic methods for structural analysis of chitin and chitosan. Mar Drugs. 2010;8(5):1567–636.
[36] Clasen SH, Müller CMO, Parize AL, Pires ATN. Synthesis and characterization of cassava starch with maleic acid derivatives by etherification reaction. Carbohydr Polym. 2018;180(May 2017):348–53. doi: 10.1016/j.carbpol.2017.10.016.
[37] Wang S, Xu J, Wang Q, Fan X, Yu Y, Wang P, et al. Preparation and rheological properties of starch-g-poly(butyl acrylate) catalyzed by horseradish peroxidase. Process Biochem. 2017;59:104–10. doi: 10.1016/j.procbio.2017.01.014.
[38] Chirani N, Yahia LH, Gritsch L, Motta FL, Chirani S, Faré S. History and applications of hydrogels. J Biomed Sci. 2015;4(2):1–23.
[39] Xu R, Xia H, He W, Li Z, Zhao J, Liu B, et al. Controlled water vapor transmission rate promotes wound-healing via wound re-epithelialization and contraction enhancement. Sci Rep. 2016;6:1–12. doi: 10.1038/srep24596.
[40] Bolton LL, Monte K, Pirone LA. Moisture and healing: beyond the jargon. Ostomy Wound Manage. 2000;46:1–6.
[41] Torres FG, Commeaux S, Troncoso OP. Starch-based biomaterials for wound-dressing applications. Starch/Staerke. 2013;65(7–8):543–51.
[42] Arun S, Kumar KAA, Sreekala MS. Fully biodegradable potato starch composites: Effect of macro and nano fiber reinforcement on mechanical, thermal and water-sorption characteristics. Int J Plast Technol. 2012;16(1):50–66.
[43] Förch R, Schönherr H. ATAJ surface design: Applications in bioscience and nanotechnology. In: Materials Today. Weinheim: Wiley-VCH; 2009. p. 471.
[44] Giridhar G, Manepalli RKNR, Apparao G. Chapter 8 – contact angle measurement techniques for nanomaterials. Thermal and Rheological Measurement Techniques for Nanomaterials Characterization. United Kingdom: Elsevier Inc; 2017. Vol. 173, p. 195. doi: 10.1016/B978-0-323-46139-9.00008-6.
[45] Unnithan AR, Sasikala ARK, Murugesan P, Gurusamy M, Wu D, Park CH, et al. Electrospun polyurethane-dextran nanofiber mats loaded with Estradiol for post-menopausal wound dressing. Int J Biol Macromol. 2015;77:1–8. doi: 10.1016/j.ijbiomac.2015.02.044.
[46] Shi R, Bi J, Zhang Z, Zhu A, Chen D, Zhou X, et al. The effect of citric acid on the structural properties and cytotoxicity of the polyvinyl alcohol/starch films when molding at high temperature. Carbohydr Polym. 2008;74(4):763–70.
[47] Li X, Weng Y, Kong X, Zhang B, Li M, Diao K, et al. A covalently crosslinked polysaccharide hydrogel for potential applications in drug delivery and tissue engineering. J Mater Sci Mater Med. 2012;23(12):2857–65.
[48] Wilson RH. Utilization and toxicity of dialdehyde- and dicarboxyl-starches. Proc Soc Exp Biol Med. 1959;102(3):735–7.
[49] Zhang X, Yang Y, Yao J, Shao Z, Chen X. Strong collagen hydrogels by oxidized dextran modification. ACS Sustain Chem Eng. 2014;2(5):1318–24. https://books.google.com.vn/books? hl = vi&lr = &id = HSnRp1m3DI4C&oi = fnd&pg = PA1&dq = xiphasia + setifer + morphology&ots = FzV5sKOfPQ&sig = SjTHQyHdWbkVwc-F5tmqPBdRoac&redir_esc = y#v = onepage&q = xiphasia setifer&f = false.
[50] Shang Y, Ding F, Xiao L, Deng H, Du Y, Shi X. Chitin-based fast responsive pH sensitive microspheres for controlled drug release. Carbohydr Polym. 2014;102(1):413–8. doi: 10.1016/j.carbpol.2013.11.039.